Microstructure and residual stress in shot peened and superfinished gearwheel teeth

M. Bandini [a], M. D'Incau [b] & P. Scardi [b]

[a] Peen Service s.r.l., via A. Pollastri 7, 40138 Bologna, Italy; [b] Department of Civil, Environmental & Mechanical Engineering, University of Trento, via Mesiano 77, 38123 Trento, Italy, e-mail: Paolo.Scardi@unitn.it

Keywords: shot peening, residual stress, residual austenite, work hardening, dislocation density

Introduction

Shot peening is acknowledged as one of the most effective treatments to increase fatigue resistance of mechanical components. A jet stream of spherical shots strikes the surface of a metallic component. The surface layers are plastically deformed whilst the underlying ones remain elastic. The main effects are the creation of a compressive residual stress field and a microstructure modification in the surface layers of the material. A side effect is usually an increase of the surface roughness.
In automotive field, superfinishing is a well-known mechanical treatment applied in order to reduce surface roughness of gearwheel teeth contact surface. In this field, surface roughness is commonly considered a key factor for lubrication, contact fatigue performance and transmission efficiency. As a rough idea, during superfinishing, workpieces are put in a vibratory tumble in conjunction with abrasive media and soap or chemical accelerant. Superfinishing is commonly considered as not effective on pre-existing compressive residual stresses.

Objectives

Compressive residual stress in surface and sub-surface regions of steel components is the most striking effect of shot-peening [2,3], nevertheless additional and significant effects concern the microstructure of the surface layers, as modifications of phase composition, crystalline domain size and lattice defect content. These features are related to plastic deformation and residual stress field, and provide further information on the effect of the surface treatment. In particular, crystalline domain size and dislocations density can be related to the work hardening process [4], providing useful information on the residual plasticity of the material, which in turn is relevant to the mechanical fatigue life of treated components. It is standard practice to use X-ray Diffraction (XRD) for the so-called X-ray Residual Stress Analysis (XRSA) [2,6] to investigate the through-thickness stress profile. It is less known, especially in the community of users and developers of surface treatments, that XRD Line Profile Analysis (LPA) can be used to investigate the microstructure of the shot-peened components. The present study has the aim to study either the effect of a superfinishing treatment (tumbling) on the residual stress profile [1] of a shot peened gear commonly obtained by the $\sin^2\psi$ method [6] or comparing information provided by X-ray diffraction line profile analysis (LPA) of extended ranges of $\theta/2\theta$ diffraction patterns [7-9].

Methodology

Cogwheels of high-strength steel were surface treated by shot-peening and tumbling after case hardening according to industrial protocols. Mechanical properties of the steel are described on the following tables:

Bulk Material			
Hardness	UTS	Yelding Stress	Elongation
590-650 HV10	1940-2160 MPa	1720 MPa	>7%

Case Hardened Material		
Depth	Hardness Line	Surface Hardness
0.6 mm	700 HV1	750-820 HV1

Two duplex shot peening treatments have been performed by means of compressed air machine. Duplex shot peening treatment is a combination of two single peening treatments where a first high intensity peening treatment is followed by a second delicate one in order to obtain a great penetration depth and a high surface compressive value at the same time.

First duplex peening treatment:

	Shot	Intensity	Coverage
1 Phase	S110 (steel cast shot)	7A	100%
2 Phase	B60 (ceramic shot)	4A	100%

Second duplex peening treatment:

	Shot	Intensity	Coverage
1 Phase	S170 (steel cast shot)	12A	100%
2 Phase	B60 (ceramic shot)	4A	100%

Gear teeth were progressively thinned as in the drawing of Figure 1 (red arrow), using a solution of nitric, phosphoric and chloric acids (90ml HCl +30ml H_3PO_4 +30ml HNO_3) at controlled temperature (35°C) under stirring (1300 rpm). At each thinning cycle, XRD data were collected according to two separate protocols: (i) $\sin^2\psi$ method, (ψ-tilt and ϕ rotation) of ferritic steel peaks (220 and 211); (ii) diffraction patterns collected over an extended angular region $\theta/2\theta$ [7-9] (orange arrows) at ϕ=0°.

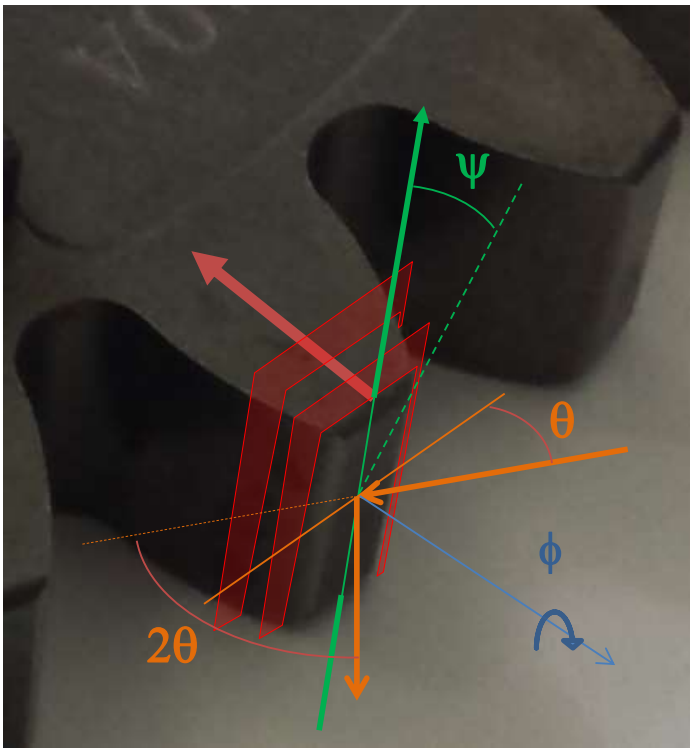

Figure 1. Schematic of progressive thinning procedure (red arrow direction) and XRD measurement geometry: ψ-tilt axis (green) and ϕ-rotation (blue) for the residual stress measurements; the equatorial plane measurements are shown with the diffraction angle θ (orange)

Data for (i) were collected on a X'Pert Panalytical instrument, equipped with a 4-circle goniometer allowing tilt and rotation of samples and $\theta/2\theta$ scansion with CoKα radiation. the diffracted beam is filtered by graphite flat-crystal monochromator before entering a conventional scintillation detector. Data for (ii) were obtained on a Thermo Xtra θ/θ diffractometer with a Bragg-Brentano geometry, using MoKα radiation. Line Profile Analysis was made according to the Whole Powder Pattern Modelling (WPPM) approach, to provide information on crystalline domain size and dislocation density: details are in the cited literature [8].

Microhardness measurements were made on cross–sectioned teeth, using a REMET HX-1000 instrument loaded with 100mN (HV0.1) for 10s, and averaging three measurement for each measured point.

Results and analysis

Residual stress after case hardening and shot peening is expected to be compressive, with the typical sub-surface peak shown in Figure 2 for sample S110B60. X-ray Elastic Constants (XECs) used in the XRSA were calculated by the Hill-Neerfeld model, i.e., as averages of XEC values from Reuss and Voigt grain interaction models [2]. Similarity of trends obtained from (211) and (220) peaks of the main *bcc* ferritic phase suggests the material behaves as a macroscopically isotropic polycrystalline solid; moreover, correspondence between measurements along two principal directions, ϕ=0° and 90°, reasonably points out the equibiaxial (i.e. rotationally symmetric) nature of the stress field.

Measurements of the (211) peak tend to be statistically more reliable than those on (220), so the former will be used in the following to compare results for different surface treatment conditions.

It is interesting to see the comparison of the above results for S110B60 with those for the same treatment after superfinishing (*superfinished* S110B60, labelled as S110B60-S). Figure 3a shows the stress trends, for ϕ=0° and 90°, in the two components. The stress trend after tumbling is similar to that of S110B60, but shifted about 20 μm toward the surface, so that maximum compression falls on the surface of the superfinished component. The microhardness profile shows the general decrease moving from the surface inward, with some difference when tumbling is used: as shown in Figure 3b for sample S110B60, the microhardness profile, like the stress profile, shifts toward the surface of the superfinished components.

Figure 3c shows that, compared to S110B60s, heavier shots push maximum compression slightly underneath the surface of S170B60-S; but the most evident difference is in the extension of compression, much deeper in S170B60-S than in S110B60-S, a feature expected for the use of heavier shots in the former case. Using a heavier shot (Figure 3d) partly compensates the effect caused by tumbling.

The WPPM analysis gives additional information on microstructure and work hardening. Extended $\theta/2\theta$ patterns collected at each layer removal step were modelled assuming a size-broadening effect from a lognormal distribution of equiaxial (i.e., spherical) scattering domains, and inhomogeneous strain-broadening from dislocations in the primary slip system of bcc iron [8,9]. The analysis also accounted for the presence of a minor fraction of retained austenite which is identified and quantified within the same procedure.

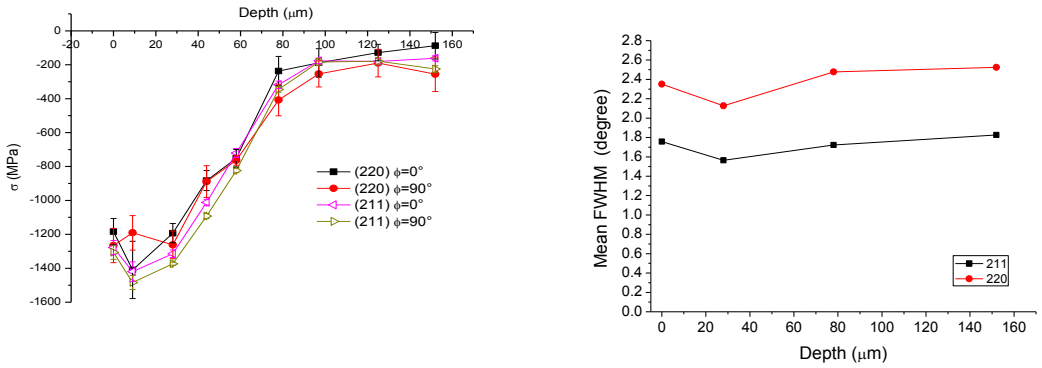

(a) (b)

Figure 2. (a) Residual stress profile from the $\sin^2\psi$ method for peaks (220) and (211) of the ferritic iron phase. (b) Corresponding mean FWHM values from $\sin^2\psi$ method.

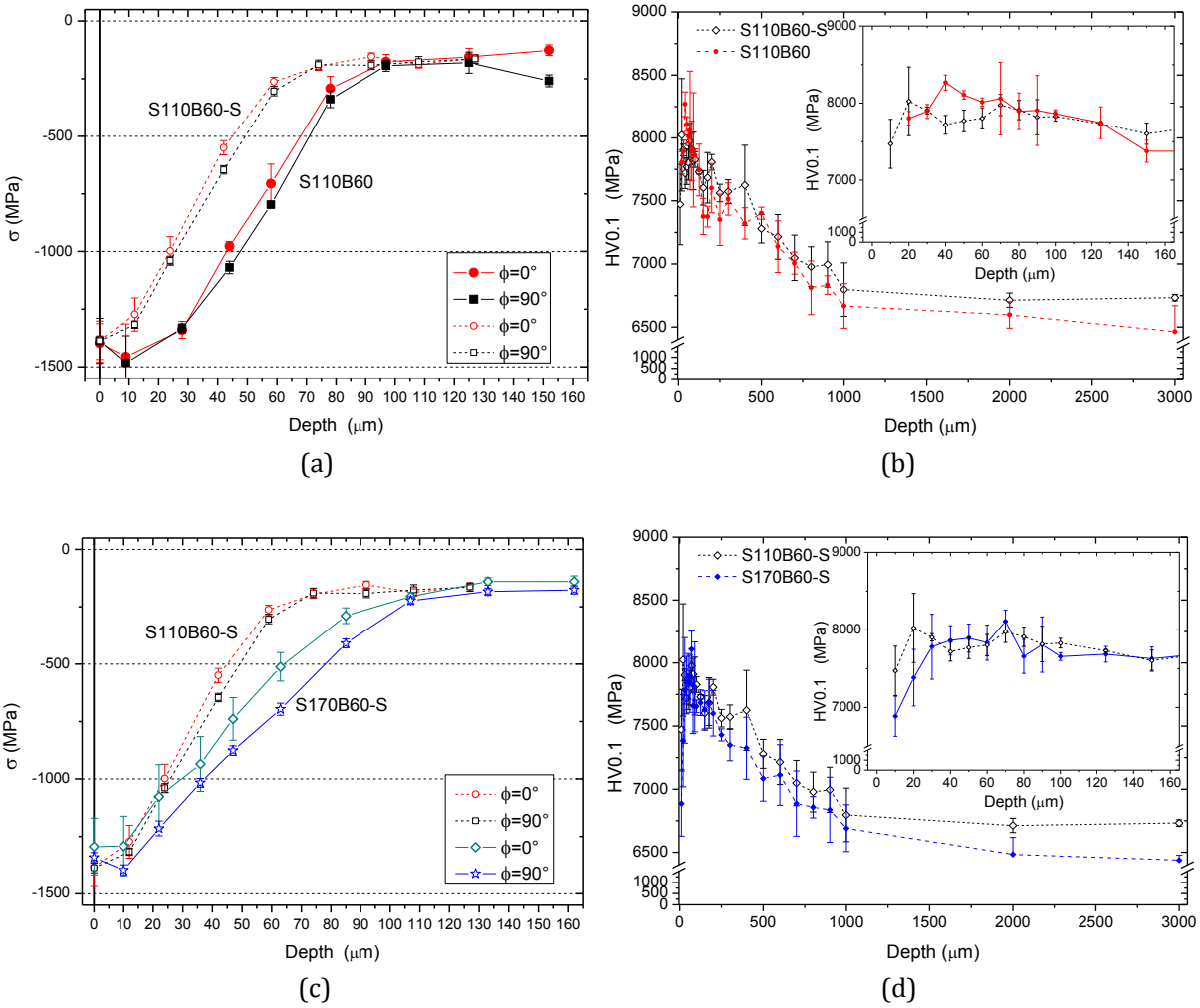

Figure 3. (a) Residual stress profile in shot-peened components S110B60-S and S110B60, respectively with and without tumbling, (b) corresponding microhardness (HV0.1) profile in MPa with detail in the inset. (c) Comparison between superfinished components S110B60-S and S170B60-S; (d) corresponding microhardness profiles with detail in the inset.

The WPPM approach was originally developed for powders [8,11], but in principle is equally applicable to any polycrystalline material. However, when analysing solid components, as in this study, the procedure must be modified to account for the effect of an intense compressive stress: owing to the elastic anisotropy of iron, diffraction peaks shift by a different amount according to the orientation of the corresponding crystallographic planes with respect to the component's surface. For this reason the stress results of Figure 3 have been used to calculate corrections of the peak positions with respect to a corresponding powder. The stress trend as a function of depth was modelled by a polynomial, the coefficients of which were refined together with the microstructural parameters of the WPPM (see below).

In the present case all $\theta/2\theta$ patterns were collected at $\phi=0°$, so the compressive stress is visible as a corresponding anisotropic expansion according to the Poisson effect. Specific details on LPA-WPPM method to account for residual stress and further investigations on the relationships between peening parameters, residual stress fields and microstructure will be described in upcoming articles by the authors.

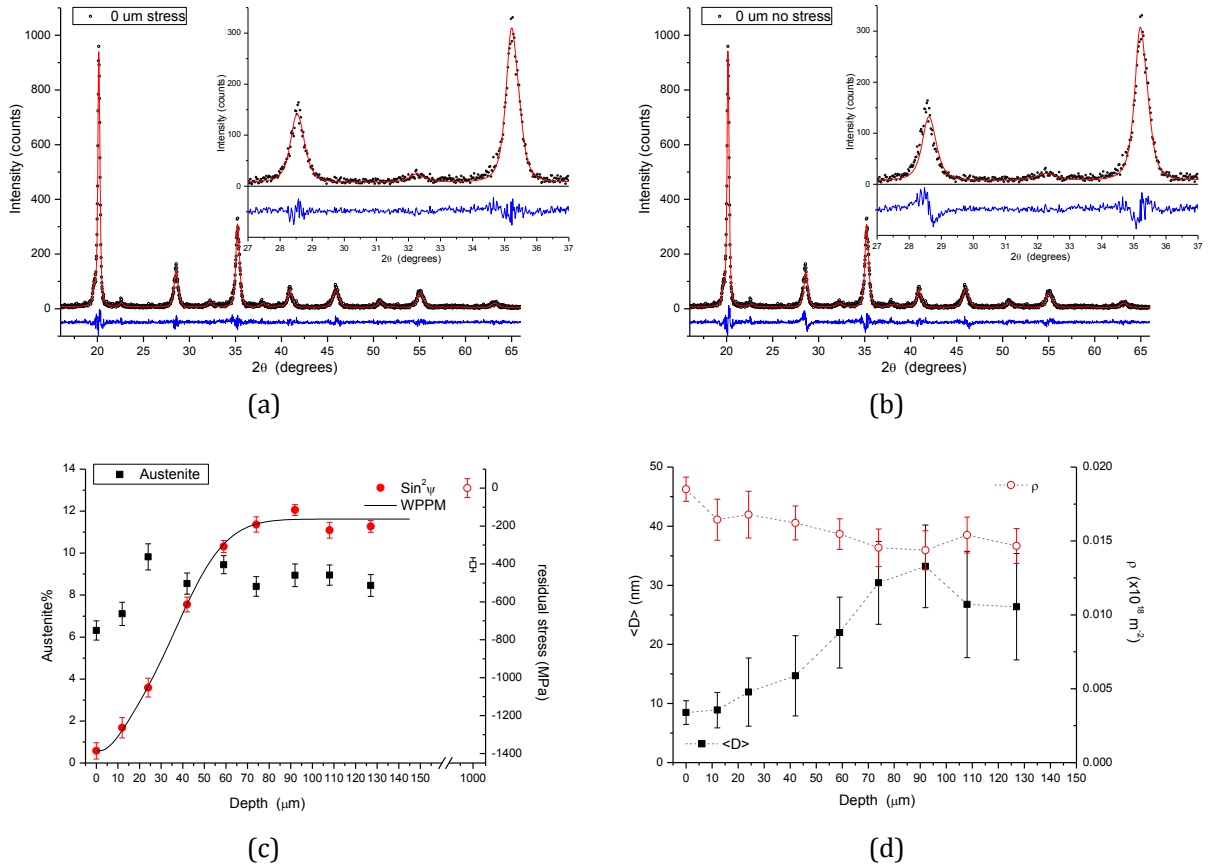

Figure 4. WPPM results for shot-peened and superfinished component S110B60-S: (a) XRD experimental data (circle), model (line) and residual (line below) for the pattern on the surface of the component (Depth=0 μm); the inset shows details of α(200), γ(220), and α(211) peaks; (b) same as (a) without compensation for the equibiaxial residual stress. (c) residual stress trend according to the the $\sin^2\psi$ method (circles, from Figure 3) with the best-fit polynomial refined by WPPM (line) together with the percentage of residual austenite; data point marked at 1000 μm corresponds to the residual austenite in the core region of the component. (d) mean crystalline domain size <D> and average dislocation density ρ.

Figure 4 shows the specific case of S110B60-S as an example of WPPM results. It is possible to see (4a-4b) that, if residual stress is not properly accounted for, no reliable modelling can be obtained of the XRD θ/2θ patterns. Figures 4c shows the residual stress values according to the $\sin^2\psi$ method (circles, from Figure 3) and the polynomial best fit from the WPPM refinement of the patterns collected at different depths. The remarkably good match was obtained due to the fast convergence and robustness of the WPPM least squares procedure [8]. Figure 4c also shows the trend of residual austenite throughout the region explored by the layer removal procedure and in the core of the component. The austenite fraction decreases on the surface, as a consequence of intense plastic deformation of shot-peening and tumbling, which transform back to ferrite part of the austenite. In Figure 4d it is possible to see the mean domain size (from a lognormal distribution) of diameters <D> and average dislocation density ρ. The former increases when moving off the compressive stress sub-surface region, where plastic deformation is highest. Dislocation density correspondingly decreases, even though the effect is much less pronounced than the variation of the domain size. Analogous trends are found for the other samples of this study, thus demonstrating a correlation between residual stress and microstructure, made evident by the XRD LPA.

LPA results and microhardness profile can provide information on the work hardening caused by the mechanical treatments and, as a consequence, on the residual plasticity of the material in the surface region. In fact, it is known that the Vicker Hardness (HV) is proportional to the yield stress (σ_y) (HV≈3σ_y

see [12] and references therein) whereas σ_y increases: (i) with the inverse of the square root of the grain size, according to the Hall-Petch relation [13, 14], and (ii) with the square root of the dislocation density, according to Taylor equation [15].

Conclusions

X-ray Diffraction can be used to gather information on the residual stress across the surface and sub-surface regions affected by surface treatments, but information can also be obtained, at the same time, on the evolution of the microstructure. As shown in this work, the expected trend of compressive stress caused by shot-peening, and the shift of the trend due to the following surface finishing by tumbling, provided by XRSA, is paralleled by similar trends of the parameters describing the microstructure. XRD Line Profile Analysis provides further data for the interpretation of the surface treatment effects in terms of size of the coherently diffracting crystalline domains, density of most relevant defects (dislocations) and residual austenite content. This information, together with the microhardness profile measured on cross-sectioned components supports an assessment of the whole microstructure and plasticity effect of the mechanical treatments.

As an effect of the strong compressive residual stress in the surface and subsurface region, the microhardness profile measured on the cross-section of the gears is determined both by the work-hardening process of shot-peening and tumbling and also partly by the marked compression induced by the same treatments. Information on plasticity only is more directly obtained from Line Profile Analysis, as the mean domain size, in some way related to grain dimension, and average dislocation density.

It worth noticing that mean FWHM values derived from XRSA in figure 2b, usually related to work hardening, provide no clear information in the present case; chemical composition (carbon content) and phase transformation (residual austenite content) gradients also contribute to FWHMs, thus making unreliable a direct interpretation of those values in terms of plasticity effects.

References

[1] R. Dusil, “On Blanking, Tumbling and Shot-Peening of Compressor Valves”, International Compressor Engineering Conference School of Mechanical Engineering, Paper 256, 1978. http://docs.lib.purdue.edu/icec/256

[2] I.C. Noyan & J.B. Cohen, Residual Stress. Measurement by diffraction and interpretation. Springer-Verlag. New York. 1987.

[3] G.S. Schajer (ed), Practical Residual Stress Measurement Methods, John Wiley & Sons, Chichester (U.K.), 2013.

[4] J. Yin, M. Umemoto, Z. G. Liu & K. Tsuchiya, Formation Mechanism and Annealing Behavior of Nanocrystalline Ferrite in Pure Fe Fabricated by Ball Milling, ISIJ International, Vol. 41 (2001), No. 11, pp. 1389–1396.

[5] M.E. Fitzpatrick & A. Lodini, Analysis of Residual Stress by Diffraction using Neutron and Synchrotron Radiation, Taylor & Francis, London, 2003.

[6] SAE HS-784. Residual Stress Measurements by X-ray Diffraction. Warrendale, PA: Society of Automotive Engineers, 2003.

[7] C.L. Azanza Ricardo, M. D'Incau, P. Scardi, Revision and extension of the standard laboratory technique for X-ray diffraction measurement of residual stress gradients, J. Appl. Cryst. 40 (2007) 675-683.

[8] P. Scardi, Powder Diffraction: Theory and Practice. chap. 14, 376–413 (Cambridge: The Royal Society of Chemistry, 2008).

[9] L. Rebuffi et al. On the reliability of powder diffraction Line Profile Analysis of plastically deformed nanocrystalline systems. Sci. Rep. 6, 20712; doi: 10.1038/srep20712 (2016).

[10] P. Scardi, S, Setti and M. Leoni, Multicapillary optics for materials science studies, Mater. Sci. Forum, 321–324 (2000) 162-167.

[11] P. Scardi & M. Leoni, Whole powder pattern modelling, Acta Cryst. A58 (2002) 190–200.

[12] M. D’Incau, M. Leoni & P. Scardi, High-energy grinding of FeMo powders, J. Mater. Research, 22 [6] (2007) 1744-1753.

[13] E.O. Hall, The deformation and ageing of mild steel: III discussion of results, Proc. Phys. Soc. London, Sect. B 64 (9) (1951) 747–753.

[14] N.J. Petch, The cleavage strength of polycrystals, J. Iron Steel Inst. 174 (1953) 25–28.

[15] G.I. Taylor, The mechanism of plastic deformation of crystals. Part I. Theoretical, Proc. R. Soc. Lond. A 145 (855) (1934) 362–387.